RSC Advances

PAPER

View Article Online
View Journal | View Issue

Cite this: *RSC Adv.*, 2021, **11**, 18870

Synthesis, optical and electrochemical properties of 4,4′-bibenzo[*c*]thiophene derivatives†

Kotaro Obayashi,[a] Keiichi Imato,[a] Satoshi Aoyama,[a] Toshiaki Enoki,[a] Seiji Akiyama,[b] Mio Ishida,[b] Seiji Suga,[c] Koichi Mitsudo[c] and Yousuke Ooyama *[a]

We designed and synthesized unsubstituted 4,4′-bibenzo[*c*]thiophene **4,4′-BBT** and its silyl-substituted derivatives **1,1′-Si-4,4′-BBT** and **1,1′,3,3′-Si-4,4′-BBT** with one or two *tert*-butyldimethylsilyl groups on each thiophene ring, as new π-building blocks in emitters, photosensitizers and semiconductors for organic optoelectronic devices. The characterization of **4,4′-BBT**, **1,1′-Si-4,4′-BBT** and **1,1′,3,3′-Si-4,4′-BBT** was successfully determined by FTIR, ^{1}H and ^{13}C NMR measurements, high-resolution mass spectrometry (HRMS) analysis, photoabsorption and fluorescence spectroscopy, cyclic voltammetry (CV) and density functional theory (DFT) calculations. Moreover, a single-crystal X-ray structural analysis was successfully made for **1,1′-Si-4,4′-BBT** and **1,1′,3,3′-Si-4,4′-BBT**. The photoabsorption and fluorescence maxima (λ_{max}^{abs} and λ_{max}^{fl}) of the three 4,4′-bibenzo[*c*]thiophene derivatives in toluene exhibit bathochromic shifts in the order of **4,4′-BBT** (359 nm and 410 nm) < **1,1′-Si-4,4′-BBT** (366 nm and 420 nm) < **1,1′,3,3′-Si-4,4′-BBT** (371 nm and 451 nm). The HOMO and LUMO energy levels rise in the order of **4,4′-BBT** (−5.55 eV and −2.39 eV) < **1,1′-Si-4,4′-BBT** (−5.45 eV and −2.34 eV) < **1,1′,3,3′-Si-4,4′-BBT** (−5.34 eV and −2.30 eV), but the rise of the HOMO energy level is larger than that of the LUMO energy level, resulting in the bathochromic shift of the photoabsorption band from **4,4′-BBT** to **1,1′,3,3′-Si-4,4′-BBT**. The fluorescence quantum yields (Φ_{fl}) of **4,4′-BBT**, **1,1′-Si-4,4′-BBT** and **1,1′,3,3′-Si-4,4′-BBT** in toluene are 0.41, 0.41 and 0.36, respectively. It is worth mentioning that in the solid state **1,1′-Si-4,4′-BBT** and **1,1′,3,3′-Si-4,4′-BBT** show relatively high $\Phi_{fl\text{-}solid}$ values of 0.22 and 0.25, respectively, whereas **4,4′-BBT** exhibits poor solid-state fluorescence properties ($\Phi_{fl\text{-}solid}$ < 0.02). This work provides an efficient synthetic method for the 4,4′-bibenzo[*c*]thiophene derivatives and their photophysical properties in the solution and solid state, electrochemical properties and X-ray crystal structures.

Received 13th February 2021
Accepted 19th May 2021

DOI: 10.1039/d1ra01189h

rsc.li/rsc-advances

Introduction

Benzo[*b*]thiophene as a π-building block has created considerable scientific interest in synthetic organic chemistry, photochemistry, electrochemistry and theoretical chemistry as well as materials chemistry, because it is an especially crucial player for functional materials due to the air-stability and commercial availability (Fig. 1).[1] Actually, benzo[*b*]thiophene derivatives are key constituents of emitters, semiconductors and photosensitizers for organic optoelectronic devices, such as organic light-emitting diodes (OLEDs),[2] organic field-effect transistors (OFETs),[3] organic photovoltaics (OPVs)[4] and dye-sensitized solar cells (DSSCs).[5] Furthermore, much effort has been made towards the construction and characterization of fused benzo[*b*]thiophene systems such as thienoacenes (*e.g.*, [1]benzothieno[3,2-*b*][1]benzothiophene (**BTBT**), dinaphtho[2,3-*b*:2′,3′-*f*]thieno[3,2-*b*]thiophene (**DNTT**) and dianthra[2,3-*b*:2′,3′-*f*]thieno[3,2-*b*]thiophene (**DATT**))[6a] and thiophene-fused naphtho[2,3-*b*:6,7-*b*]dithiophene diimide (**NDTI**)[6b] in the past two decades. Indeed, these benzo[*b*]thiophene derivatives have been used as organic semiconductors with high carrier mobility and stability under ambient conditions. Similarly, benzo[*c*]thiophene is also an interesting π-building block (Fig. 1). For example, Wudl and Heeger have prepared poly(1,3-benzo[*c*]thiophene) (*i.e.*, poly(-isothianaphthene) (**PITN**)) and demonstrated that **PITN** can form the aromatic and quinoidal states by the bond alternation.[7] In the aromatic state, the benzo[*c*]thiophene unit contains a thiophene ring in the structure. On the other hand, in the quinoidal state, the unit contains the more stable benzene ring in the structure. Thus, **PITN** has a low band gap (E_g = 1.0–1.2 eV), which is about 1.0 eV lower than that of polythiophene (**PT**), because the polymer backbone of **PITN** intrinsically stabilizes its quinoidal state,

[a]*Department of Applied Chemistry, Graduate School of Engineering, Hiroshima University, 1-4-1 Kagamiyama, Higashi-Hiroshima 739-8527, Japan. E-mail: yooyama@hiroshima-u.ac.jp; Fax: +81 82-424-5494*

[b]*Science & Innovation Center, Mitsubishi Chemical Corporation, 1000, Kamoshida-cho, Aoba-ku, Yokohama-shi, Kanagawa 227-8502, Japan*

[c]*Division of Applied Chemistry, Graduate School of Natural Science and Technology, Okayama University, 3-1-1 Tsushima-naka, Kita-ku, Okayama 700-8530, Japan*

† Electronic supplementary information (ESI) available. CCDC [2055734, 2055735]. For ESI and crystallographic data in CIF or other electronic format see DOI: 10.1039/d1ra01189h

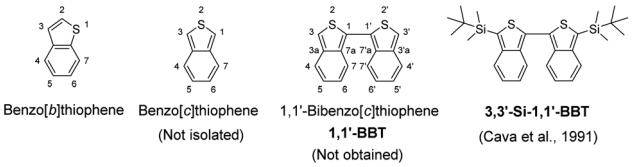

Fig. 1 Chemical structures of benzo[*b*]thiophene, benzo[*c*]thiophene, 1,1′-bibenzo[*c*]thiophene **1,1′-BBT** and 3,3′-silyl-disubstituted-1,1′-bibenzo[*c*]thiophene **3,3′-Si-1,1′-BBT**.

that is, the contribution of the quinoidal state decreases the E_g. However, unsubstituted benzo[*c*]thiophene has never been isolated so far due to the instability in air, in contrast to unsubstituted benzo[*b*]thiophene. Nevertheless, some benzo[*c*]thiophene derivatives with substituents on the thiophene ring and/or the benzene ring such as 1,3-diarylbenzo[*c*]thiophenes,[8–12] 5,6-disubstituted benzo[*c*]thiophenes[13] and 1,3,4,7- or 1,3,5,6-tetrasubstituted benzo[*c*]thiophenes[14–16] have been synthesized and their optical and electrochemical properties were investigated, although much less substituted benzo[*c*]thiophene derivatives have been reported than substituted benzo[*b*]thiophene derivatives. In particular, few 3,3′-disubstituted-1,1′-bibenzo[*c*]thiophenes as the 1,1′-dimer of bibenzo[*c*]thiophene have been developed by Cava,[17] Mohanakrishnan[18] and Ono *et al.*,[19] and they revealed their synthetic methods and, optical and electrochemical properties, although there are no reports on the synthesis and physical properties of unsubstituted 1,1′-bibenzo[*c*]thiophene **1,1′-BBT** (Fig. 1). On the other hand, in our previous work,[20] we have designed and developed 1,1′-bis(*tert*-butyldimethylsilyl)-4,4′-bibenzo[*c*]thiophene (**1,1′-Si-4,4′-BBT**) as the 4,4′-dimer of bibenzo[*c*]thiophene and the fused-bibenzo[*c*]thiophene (**PHDT-Si**), which is the first report on the synthesis, characterization and optical and electrochemical properties of 4,4′-bibenzo[*c*]thiophene and fused-bibenzo[*c*]thiophene derivatives (Fig. 2). **PHDT-Si** exhibits intense vibronic-structured photoabsorption (λ_{max}^{abs} = 598 nm, molar extinction coefficient (ε_{max}) = 80 900 M^{-1} cm^{-1} in toluene) and fluorescence (λ_{max}^{fl} = 613 nm, fluorescence quantum yield (Φ_{fl}) = 0.74 in toluene) bands in a significantly longer wavelength region and a smaller Stokes shift (409 cm^{-1}), compared to those of **1,1′-Si-4,4′-BBT** (λ_{max}^{abs} = 366 nm, λ_{max}^{fl} = 420 nm, ε_{max} = 14 400 M^{-1} cm^{-1}, Φ_{fl} = 0.41, Stokes shift = 3513 cm^{-1} in toluene). It is worth noting here that **1,1′-Si-4,4′-BBT** exhibits the λ_{max}^{abs} in a shorter wavelength region by 40 nm in comparison with that of the isomer 3,3′-bis(*tert*-butyldimethylsilyl)-1,1′-bibenzo[*c*]thiophene **3,3′-Si-1,1′-BBT** (λ_{max}^{abs} = 406 nm, ε_{max} = *ca.* 11 500 M^{-1} cm^{-1} in CH_2Cl_2) reported by Cava *et al.*[17a] However, in order to use extensively and commonly benzo[*c*]thiophene derivatives as π-building blocks in the emitters, photosensitizers and semiconductors for organic optoelectronic devices, it is necessary to develop efficient and facile synthetic methods for benzo[*c*]thiophene derivatives.

Therefore, the aim of this work is to provide the synthetic strategy for 4,4′-bibenzo[*c*]thiophene derivatives and to reveal their optical and electrochemical properties. With this aim, we designed and synthesized unsubstituted 4,4′-bibenzo[*c*]thiophene (**4,4′-BBT**: abbr. as **BBT-1**) and its silyl-substituted derivatives **1,1′,3,3′-Si-4,4′-BBT** (abbr. as **BBT-3**) with two sterically hindered *tert*-butyldimethylsilyl groups on each thiophene ring as well as **1,1′-Si-4,4′-BBT** (abbr. as **BBT-2**) (Fig. 2). The characterization of **BBT-1**, **BBT-2** and **BBT-3** was successfully determined by FTIR, ^1H and ^{13}C NMR measurements, high-resolution mass spectrometry (HRMS) analysis, photoabsorption and fluorescence spectroscopy, cyclic voltammetry (CV) and density functional theory (DFT) calculations. This work is the first to achieve the synthesis, photophysical and electrochemical characteristics of unsubstituted 4,4′-bibenzo[*c*]thiophene **BBT-1**. Moreover, we achieved the single-crystal X-ray structural analysis of **BBT-2** and **BBT-3**. Herein we report an efficient synthetic method for the 4,4′-bibenzo[*c*]thiophene derivatives and their photophysical properties in the solution and the solid state, electrochemical properties and X-ray crystal structures.

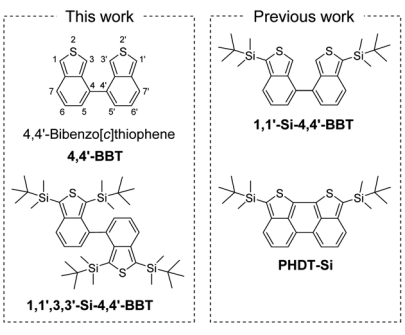

Fig. 2 Chemical structures of 4,4′-bibenzo[*c*]thiophene **4,4′-BBT** (**BBT-1**), 1,1′-silyl-disubstituted-4,4′-bibenzo[*c*]thiophene **1,1′-Si-4,4′-BBT** (**BBT-2**), 1,1′,3,3′-silyl-tetrasubstituted-4,4′-bibenzo[*c*]thiophene **1,1′,3,3′-Si-4,4′-BBT** (**BBT-3**) and fused-bibenzo[*c*]thiophene **PHDT-Si**.

Results and discussion

Synthesis

4,4′-Bibenzo[*c*]thiophene (**BBT-1**) and its silyl-substituted derivatives (**BBT-2** and **BBT-3**) were synthesized according to a stepwise synthetic protocol (Scheme 1). Indeed, unsubstituted 4,4′-bibenzo[*c*]thiophene (**BBT-1**) was successfully prepared by treatment of 1,1′,3,3′-tetrahydro-[4,4′-bibenzo[*c*]thiophene] 2,2′-

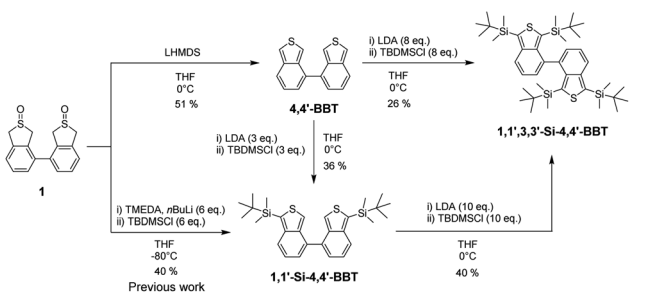

Scheme 1 Synthetic route to 4,4′-bibenzo[*c*]thiophene derivatives **4,4′-BBT** (**BBT-1**), **1,1′-Si-4,4′-BBT** (**BBT-2**) and **1,1′,3,3′-Si-4,4′-BBT** (**BBT-3**).

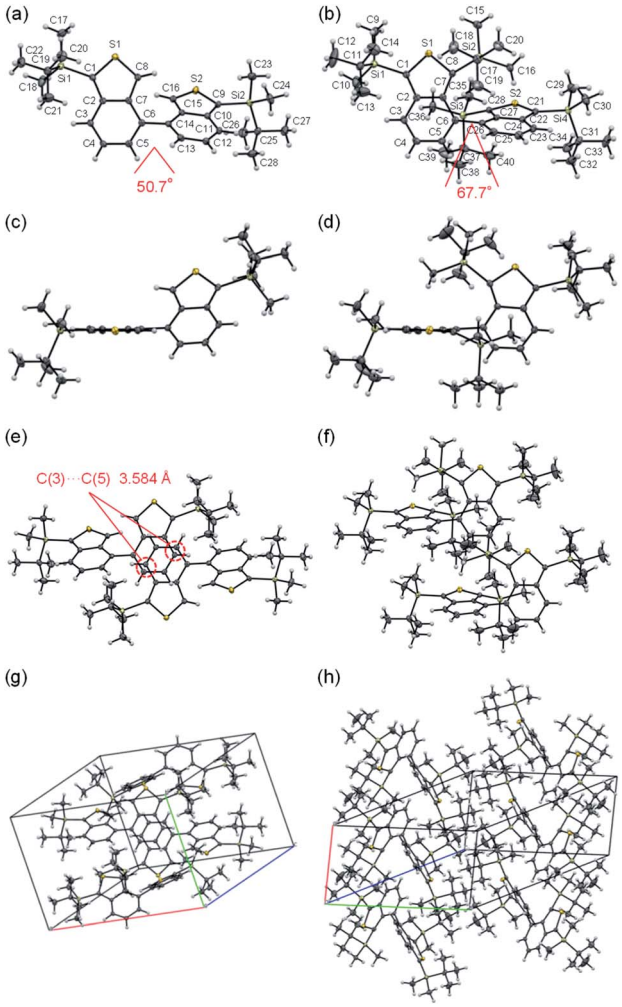

Fig. 3 Crystal structures of 1,1′-Si-4,4′-BBT (BBT-2) and 1,1′,3,3′-Si-4,4′-BBT (BBT-3): (a) top view, (c) side view, (e) a top view of the pair of molecules and (g) molecular packing structure of BBT-2, and (b) top view, (d) side view, (f) a top view of the pair of molecules and (h) molecular packing structure of BBT-3.

dioxide 1 (see ref. 20 for the synthesis) with lithium hexamethyldisilazide (LHMDS). In our previous work, we demonstrated that **BBT-2** with a *tert*-butyldimethylsilyl group on each thiophene ring was obtained by the reaction of 1 with tetramethylethylenediamine (TMEDA) and then *n*BuLi, followed by treatment with *tert*-butyldimethylsilyl chloride (TBDMSCl).[20] In this work, we found that **BBT-2** was also prepared by the reaction of **BBT-1** with lithium diisopropylamide (LDA), followed by treatment with TBDMSCl. It is worth noting here that the above reactions from 1 or **BBT-1** did not yield 3,3′-Si-4,4′-BBT with two *tert*-butyldimethylsilyl groups at the 3,3′-positions. This result indicates that the lithiation of **BBT-1** preferentially occurs at the 1,1′-positions rather than the 3,3′-positions. On the other hand, **BBT-3** was not obtained directly from 1 even under the condition using TMEDA, *n*BuLi (10 eq.) and then TBDMSCl (10 eq.). Finally, we prepared **BBT-3** with two *tert*-butyldimethylsilyl groups on each thiophene ring by the reaction of **BBT-1** or **BBT-2** with LDA, followed by treatment with TBDMSCl. The characterization of **BBT-1**, **BBT-2** and **BBT-3** was successfully determined by FTIR, ^{1}H and ^{13}C NMR measurements and HRMS analysis. Therefore, this result proposes the stepwise synthetic method for the introduction of substituents into the thiophene rings of the 4,4′-bibenzo[*c*]thiophene skeleton.

X-ray crystal structures

A single-crystal X-ray structural analysis was successfully made for **BBT-2** and **BBT-3** (Fig. 3), while unfortunately, we could not obtain single crystals of **BBT-1** with sufficient size to make the X-ray structural analysis possible. The dihedral angles between the two benzo[*c*]thiophene units in **BBT-2** and **BBT-3** are 50.7° and 67.7° (Fig. 3a–d), respectively, which show that the two units in **BBT-3** twist considerably due to the steric hindrance of the *tert*-butyldimethylsilyl groups at the 3,3′-positions, compared to those in **BBT-2**. The crystal structure of **BBT-2** is made up of dimer units composed of pairs of molecules (Fig. 3e and g). There are two short interatomic contacts of less than 3.60 Å between a pair of molecules, that is, the interatomic distance between C(3) in a benzo[*c*]thiophene unit and C(5) in the other unit is *ca.* 3.58 Å. In the crystal structure of **BBT-3**, on the other hand, there are no short π–π contacts of less than 3.60 Å between the neighboring molecules (Fig. 3f and h), which indicates the absence of the π–π interactions between the molecules.

Photophysical properties in the solution and the solid state

The photoabsorption and fluorescence spectra of **BBT-1**, **BBT-2** and **BBT-3** in toluene are shown in Fig. 4a, and their photophysical data are summarized in Table 1. The photoabsorption spectra demonstrated that **BBT-2** and **BBT-3** exhibit an intense photoabsorption band (λ_{max}^{abs} = 366 nm and 371 nm, respectively) with a relatively high ε_{max} value (14 400 M^{-1} cm^{-1} and 21 300 M^{-1} cm^{-1}, respectively) in a longer wavelength region by 7 nm and 12 nm, respectively, in comparison with that of **BBT-1** (λ_{max}^{abs} = 359 nm, ε_{max} = 7500 M^{-1} cm^{-1}), due to the electron-donating *tert*-butyldimethylsilyl group. The corresponding fluorescent bands of the three fluorophores appear in longer wavelength regions in the order of **BBT-1** (λ_{max}^{fl} = 410 nm) < **BBT-2** (λ_{max}^{fl} = 420 nm) < **BBT-3** (λ_{max}^{fl} = 451 nm), and thus, the Stokes

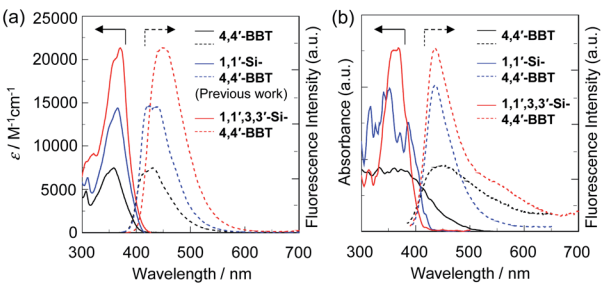

Fig. 4 (a) Photoabsorption (solid line) and fluorescence (dotted line) spectra of 4,4′-BBT (BBT-1), 1,1′-Si-4,4′-BBT (BBT-2) and 1,1′,3,3′-Si-4,4′-BBT (BBT-3) in toluene. (b) Solid-state UV-vis diffuse reflection–absorption (solid line) and fluorescence (dotted line) spectra (λ^{ex} = 360 nm) of the as-recrystallized BBT-1, BBT-2 and BBT-3.

Table 1 Photophysical and electrochemical data and HOMO and LUMO energy levels of 4,4′-bibenzo[*c*]thiophene derivatives in the solution

Dye	λ_{max}^{abs} [a]/nm (ε_{max}/M^{-1} cm^{-1})	λ_{max}^{fl} [b]/nm (Φ_{fl})	τ_{fl} [c]/ns	k_r [d]/s^{-1}	k_{nr} [e]/s^{-1}	k_{nr}/k_r	E_{onset}^{ox} [f]/V	E_g^{optg}/eV	HOMO[h]/eV	LUMO[h]/eV
4,4′-BBT	359 (7500)	410 (0.41)	3.46	1.18×10^8	1.70×10^8	1.44	0.75	3.16	−5.55	−2.39
1,1′-Si-4,4′-BBT	366 (14 400)[i]	420 (0.41)[i]	3.19[i]	1.29×10^8[i]	1.84×10^8[i]	1.43[i]	0.65[i]	3.11[i]	−5.45[i]	−2.34[i]
1,1′,3,3′-Si-4,4′-BBT	371 (21 300)	451 (0.36)	3.59	1.00×10^8	1.78×10^8	1.78	0.54	3.04	−5.34	−2.30

[a] In toluene. [b] In toluene. Fluorescence quantum yields (Φ_{fl}) were determined by using a calibrated integrating sphere system (λ^{ex} = 359 nm, 366 nm and 371 nm for **4,4′-BBT** (**BBT-1**), **1,1′-Si-4,4′-BBT** (**BBT-2**) and **1,1′,3,3′-Si-4,4′-BBT** (**BBT-3**), respectively). [c] Fluorescence lifetime. [d] Radiative rate constant ($k_r = \Phi_{fl}/\tau_{fl}$). [e] Nonradiative rate constant ($k_{nr} = (1 - \Phi_{fl})/\tau_{fl}$). [f] Onset ($E_{onset}^{ox}$) *versus* Fc/Fc$^+$ of the oxidation potential. [g] Optical energy gaps (E_g^{opt}) were determined from the intersection (393 nm, 399 nm and 408 nm for **BBT-1**, **BBT-2** and **BBT-3**, respectively) of photoabsorption and fluorescence spectra in toluene. [h] *Versus* vacuum level. [i] Previous work (ref. 20).

shift (SS) values increase in the order of **BBT-1** (3465 cm^{-1}) ≈ **BBT-2** (3513 cm^{-1}) < **BBT-3** (4781 cm^{-1}). The Φ_{fl} values of **BBT-1**, **BBT-2** and **BBT-3** are 0.41, 0.41 and 0.36, respectively, indicating moderate fluorescence properties. The relatively low Φ_{fl} and large SS values of **BBT-3** indicate significant changes in the molecular and electronic structures between the ground and excited states by the rotation or twisting of the two benzo[*c*]thiophene units, due to the steric hindrance of the *tert*-butyldimethylsilyl groups at the 3,3′-positions. The time-resolved fluorescence spectroscopy of the three fluorophores demonstrated that the fluorescence lifetimes (τ_{fl}) are 3.46 ns for **BBT-1**, 3.19 ns for **BBT-2** and 3.59 ns for **BBT-3**, and thus, there are little difference in the τ_{fl} values between the three fluorophores. The radiative rate constant ($k_r = 1.00 \times 10^8$ s^{-1}) for **BBT-3** is slightly smaller than those (1.18×10^8 s^{-1} and 1.29×10^8 s^{-1}, respectively) for **BBT-1** and **BBT-2**. In contrast, the nonradiative rate constants (k_{nr} = 1.70–1.84 × 10^8 s^{-1}) of the three fluorophores resemble each other. Consequently, the ratio of nonradiative constant to radiative constant ($k_{nr}/k_r = 1.78$) for **BBT-3** is larger than those (1.44 and 1.43, respectively) for **BBT-1** and **BBT-2**, suggesting that the lower Φ_{fl} value of **BBT-3** is mainly due to the smaller k_r value compared to those of **BBT-1** and **BBT-2**.

In order to investigate the solid-state photophysical properties of **BBT-1**, **BBT-2** and **BBT-3**, we have measured the solid-state UV-Vis diffuse reflection–photoabsorption and fluorescence spectra for the solids (Fig. 4b), and their photophysical data are summarized in Table 2. Both **BBT-2** and **BBT-3** in the solid state show a photoabsorption band at around 360 nm with an onset at 420–425 nm, which is similar to the corresponding photoabsorption band of the two fluorophores in toluene (Fig. 4a). On the other hand, the photoabsorption band of **BBT-1** in the solid state is broadened in a longer wavelength region with an onset of *ca.* 500 nm, in comparison with that in toluene. The corresponding solid-state fluorescence spectra revealed that **BBT-1** and **BBT-2** show a fluorescence band ($\lambda_{max}^{fl\text{-}solid}$ = 455 nm and 435 nm, respectively) in a longer wavelength region by 45 nm and 15 nm, respectively, compared to those in toluene. It is worth mentioning here that the fluorescence band ($\lambda^{fl\text{-}solid}{}_{max}$ = 435 nm) of **BBT-3** in the solid state appeared in a shorter wavelength region than that (λ_{max}^{fl} = 451 nm) in toluene (Fig. 4a). The $\Phi_{fl\text{-}solid}$ values of **BBT-1**, **BBT-2** and **BBT-3** in the solid state are <0.02, 0.22 and 0.25, respectively, which are lower than those in toluene (Table 1). In particular, the fluorescence properties of **BBT-1** were strongly quenched in the solid state. The bathochromic shifts of λ_{max}^{abs} and λ_{max}^{fl} and the lowering of Φ_{fl} value by changing from the solution to the solid state are quite common and explained in terms of the formation of intermolecular π–π interactions between the fluorophores in the solid state and consequent delocalization of excitons or excimers.[21] Thus, for **BBT-1**, the bathochromic shift of λ_{max}^{fl} and the significant lowering of Φ_{fl} value by changing from the solution to the solid state would be attributed to the formation of intermolecular π–π interactions between the fluorophores in the solid state. On the other hand, the relatively high $\Phi_{fl\text{-}solid}$ value of **BBT-3** in the solid state is based on the fact that the short π–π contacts of less than 3.60 Å between the neighboring molecules were not observed in the crystal structure of **BBT-3** (Fig. 3f), which indicates the absence of the intermolecular π–π interactions between the fluorophores. Indeed, the four *tert*-butyldimethylsilyl groups at the 1,1′,3,3′-positions can effectively prevent the fluorophores from forming intermolecular π–π interactions in the solid state. In addition, for **BBT-3**, the

Table 2 Photophysical data of 4,4′-bibenzo[*c*]thiophene derivatives in the solid state

Dye	$\lambda_{max}^{abs\text{-}solid}$/nm	$\lambda_{max}^{fl\text{-}solid}$[a]/nm ($\Phi_{fl\text{-}solid}$)	$\tau_{fl\text{-}solid}$ [b]/ns	$k_{r\text{-}solid}$ [c]/s^{-1}	$k_{nr\text{-}solid}$ [d]/s^{-1}	$k_{nr\text{-}solid}/k_{r\text{-}solid}$
4,4′-BBT (**BBT-1**)	360	455 (<0.02)	<1	—[e]	—[e]	—[e]
1,1′-Si-4,4′-BBT (**BBT-2**)	360	435 (0.22)	1.61	1.38×10^8	4.84×10^8	3.55
1,1′,3,3′-Si-4,4′-BBT (**BBT-3**)	370	435 (0.25)	2.33	9.00×10^7	3.38×10^8	3.76

[a] Fluorescence quantum yields ($\Phi_{fl\text{-}solid}$) were determined by using a calibrated integrating sphere system (λ^{ex} = 360 nm for **4,4′-BBT** (**BBT-1**), **1,1′-Si-4,4′-BBT** (**BBT-2**) and **1,1′,3,3′-Si-4,4′-BBT** (**BBT-3**)). [b] Fluorescence lifetime. [c] Radiative rate constant ($k_{r\text{-}solid} = \Phi_{fl\text{-}solid}/\tau_{fl\text{-}solid}$). [d] Nonradiative rate constant ($k_{nr\text{-}solid} = (1 - \Phi_{fl\text{-}solid})/\tau_{fl\text{-}solid}$). [e] Due to feeble solid-state fluorescence properties.

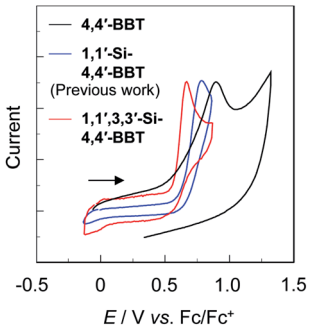

Fig. 5 Cyclic voltammograms of 4,4′-BBT (BBT-1), 1,1′-Si-4,4′-BBT (BBT-2) and 1,1′,3,3′-Si-4,4′-BBT (BBT-3) in acetonitrile containing 0.1 M Bu_4NClO_4 at a scan rate of 100 mV s^{-1}. The arrow denotes the direction of the potential scan.

hypsochromic shift of λ_{max}^{fl} by changing from the solution to the solid state may be attributed to inhibition of structural relaxation in the excited state by restriction of the rotation or twisting of the two benzo[*c*]thiophenes in the solid state, due to the steric hindrance of the *tert*-butyldimethylsilyl groups at the 3,3′-positions between the neighboring fluorophores. The time-resolved fluorescence spectroscopy of the three 4,4′-bibenzo[*c*]thiophene derivatives in the solid state demonstrated that the $\tau_{fl\text{-}solid}$ values are 1.61 ns for **BBT-2** and 2.33 ns for **BBT-3**, which are shorter than those (3.19 ns and 3.59 ns, respectively) in toluene. However, the precise evaluation of the $\tau_{fl\text{-}solid}$ value (<1 ns) of **BBT-1** was difficult due to its feeble solid-state fluorescence properties. The $k_{r\text{-}solid}$ values for **BBT-2** and **BBT-3** in the solid state are 1.38×10^8 s^{-1} and 9.00×10^7 s^{-1}, respectively, which are almost equivalent to those (1.29×10^8 s^{-1} and 1.00×10^8 s^{-1}, respectively) in toluene. In contrast, the $k_{nr\text{-}solid}$ values (4.84×10^8 s^{-1} and 3.38×10^8 s^{-1}, respectively) for **BBT-2** and **BBT-3** in the solid state are larger than those (1.84×10^8 s^{-1} and 1.78×10^8 s^{-1}, respectively) in toluene. The $k_{nr\text{-}solid}/k_{r\text{-}solid}$ values for **BBT-2** and **BBT-3** in the solid state are 3.55 and 3.76, respectively, which are larger than those (1.43 and 1.78, respectively) in toluene, suggesting that the non-radiative decay in the solid state is accelerated. Consequently, the relatively low $\Phi_{fl\text{-}solid}$ values of **BBT-2** and **BBT-3** in the solid state are mainly due to the larger $k_{nr\text{-}solid}$ values compared to those in toluene.

Electrochemical properties

The electrochemical properties of **BBT-1**, **BBT-2** and **BBT-3** were determined using CV in acetonitrile containing 0.1 M tetrabutylammonium perchlorate (Bu_4NClO_4). The potentials were internally referenced to ferrocene/ferrocenium (Fc/Fc^+). The cyclic voltammograms of the three compounds are shown in Fig. 5, and their electrochemical data and the HOMO and LUMO energy levels are summarized in Table 1. For all the three compounds, an irreversible oxidation wave was observed at 0.88 V for **BBT-1**, 0.78 V for **BBT-2** and 0.67 V for **BBT-3**, while any obvious reduction wave did not appear within the potential window. The oxidation waves for **BBT-2** and **BBT-3** are cathodically shifted by 0.10 V and 0.21 V, respectively, compared to that for **BBT-1**, indicating that the introduction of the *tert*-butyldimethylsilyl group into the benzo[*c*]thiophene skeleton can lower the oxidation potential. The HOMO energy levels ($-[E_{onset}^{ox} + 4.8]$ eV) *versus* vacuum level were estimated from the onset potentials ($E_{onset}^{ox} = 0.75$ V for **BBT-1**, 0.65 V for **BBT-2** and 0.54 V for **BBT-3**) of the oxidation waves, and the LUMO energy levels were estimated from the E_{onset}^{ox} and intersections (optical energy gap: $E_g^{opt} = 3.16$ eV for **BBT-1**, 3.11 eV for **BBT-2** and 3.04 eV for **BBT-3**) of the photoabsorption and fluorescence spectra in toluene. The HOMO energy level rises in the order of **BBT-1** (−5.55 eV) < **BBT-2** (−5.45 eV) < **BBT-3** (−5.34 eV).

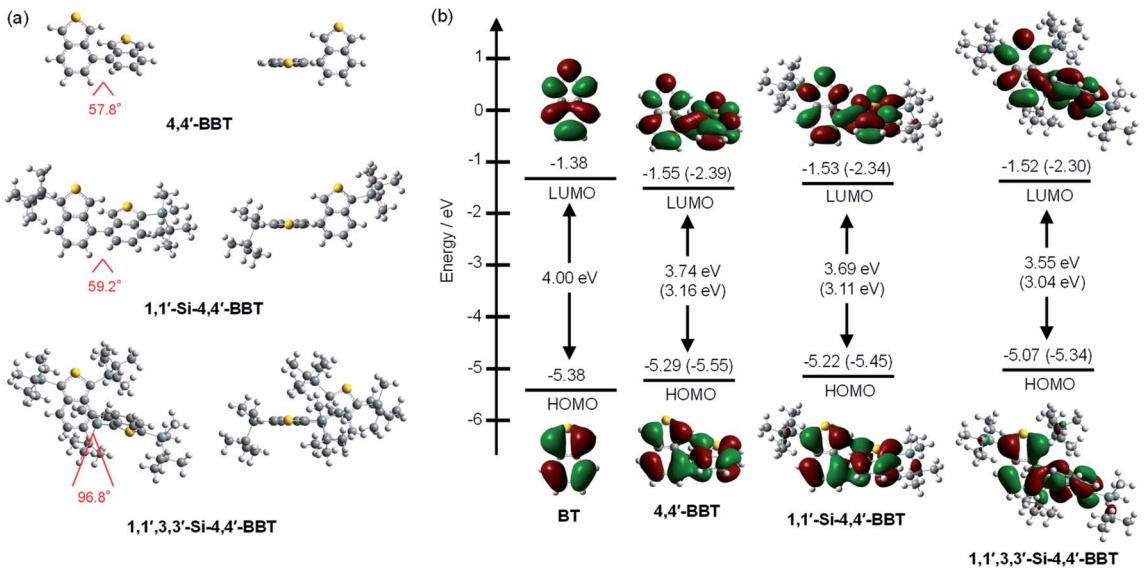

Fig. 6 (a) Optimized geometries (top and side views) of 4,4′-BBT (BBT-1), 1,1′-Si-4,4′-BBT (BBT-2) and 1,1′,3,3′-Si-4,4′-BBT (BBT-3) and (b) energy level diagram, HOMO and LUMO of BT and the three 4,4′-bibenzo[c]thiophene derivatives derived from DFT calculations at the B3LYP/6-31G(d,p) level. Numbers in parentheses are the experimental values.

Similarly, the LUMO energy level rises in the order of **BBT-1** (−2.39 eV) < **BBT-2** (−2.34 eV) < **BBT-3** (−2.30 eV). However, from **BBT-1** to **BBT-3**, the rise of the HOMO energy level is larger than that of the LUMO energy level. Consequently, the fact reveals that the bathochromic shift of the photoabsorption band from **BBT-1** to **BBT-2** and **BBT-3** is mainly attributed to the destabilization of the HOMO energy level through the introduction of the electron-donating *tert*-butyldimethylsilyl group into the benzo[*c*]thiophene skeleton, resulting in a decrease in the HOMO–LUMO band gap.

Theoretical calculations

In order to examine the electronic structures of the 4,4′-bibenzo[*c*]thiophene derivatives, the molecular structures and molecular orbitals of **BBT-1**, **BBT-2** and **BBT-3** and benzo[*c*]thiophene (**BT**) as a reference were calculated using DFT at the B3LYP/6-31G(d,p) level[22] (Fig. 6). The DFT calculations demonstrate that the calculated dihedral angles between the two benzo[*c*]thiophene units are 57.8° for **BBT-1**, 59.2° for **BBT-2** and 96.8° for **BBT-3**, that is, the two units in **BBT-3** twist considerably due to the *tert*-butyldimethylsilyl groups at the 3,3′-positions, compared to those in **BBT-1** and **BBT-2** (Fig. 6a). Therefore, good correlation was observed between the molecular structures estimated by the DFT calculations and experimentally obtained from the X-ray crystal structure analysis, although for **BBT-3**, the calculated dihedral angle between the two benzo[*c*]thiophene units is larger than that determined from the X-ray crystal structure analysis (Fig. 3a and b). As shown in Fig. 6b, for the three 4,4′-bibenzo[*c*]thiophene derivatives the HOMO are delocalized on each benzo[*c*]thiophene unit, as with the pattern of **BT**. However, the LUMO for the three 4,4′-bibenzo[*c*]thiophene derivatives are delocalized over the whole molecule through the 4,4′-positions. It was found that the HOMO energy levels of the three 4,4′-bibenzo[*c*]thiophene derivatives are higher than that (−5.38 eV) of **BT**, but their LUMO energy levels are lower than that (−1.38 eV) of **BT**. The HOMO and LUMO energy levels rise in the order of **BBT-1** (−5.29 eV and −1.55 eV) < **BBT-2** (−5.22 eV and −1.53 eV) < **BBT-3** (−5.07 eV and −1.52 eV), while from **BBT-1** to **BBT-3**, the rise of the HOMO energy level is larger than that of the LUMO energy level, resulting in a decrease in the HOMO–LUMO band gap. Moreover, the time-dependent density functional theory (TD-DFT) calculations indicate that the calculated $\lambda_{max}^{abs\text{-}calcd}$ of **BBT-1**, **BBT-2** and **BBT-3** is 345 nm, 354 nm and 356 nm, respectively, which appears in a significantly longer wavelength region than that (332 nm) of **BT** (Fig. 7). For **BT** and the three 4,4′-bibenzo[*c*]thiophene derivative, the $S_0 \rightarrow S_1$ transitions are mainly attributed to the transitions from the HOMO to the LUMO (70% for **BT**, 67% for **BBT-1**, 67% for **BBT-2** and 68% for **BBT-3**). The corresponding oscillator strength (*f*) value increases in the order of **BT** (0.07) < **BBT-1** (0.11) < **BBT-3** (0.14) < **BBT-2** (0.16), and indeed, the calculated ε_{calcd} value also increases in the order of **BT** (3000 M^{-1} cm^{-1}) < **BBT-1** (7800 M^{-1} cm^{-1}) < **BBT-3** (13 200 M^{-1} cm^{-1}) < **BBT-2** (15 600 M^{-1} cm^{-1}). Thus, the DFT calculations reveal that the bathochromic shift of the photoabsorption band from **BBT-1** to **BBT-2** and **BBT-3** is ascribable to the destabilization of the HOMO energy level through the introduction of the electron-donating *tert*-butyldimethylsilyl group into the benzo[*c*]thiophene skeleton. Consequently, the DFT calculations are in good agreement with the experimental results from the CV and the photoabsorption and fluorescence spectral analyses, although the *f* and ε_{calcd} values of **BBT-3** are slightly lower than those of **BBT-2**, which is opposite in the values to the experimental results.

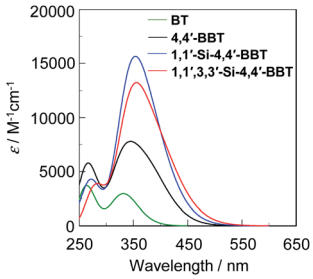

Fig. 7 Photoabsorption spectra of BT, 4,4′-BBT (BBT-1), 1,1′-Si-4,4′-BBT (BBT-2) and 1,1′,3,3′-Si-4,4′-BBT (BBT-3) derived from TD-DFT calculations.

Conclusions

We have achieved a facile synthesis of 4,4′-bibenzo[*c*]thiophene derivatives, unsubstituted 4,4′-bibenzo[*c*]thiophene **4,4′-BBT** and its silyl-substituted derivatives **1,1′-Si-4,4′-BBT** and **1,1′,3,3′-Si-4,4′-BBT** with one or two *tert*-butyldimethylsilyl groups on each thiophene ring, and revealed their photophysical properties in the solution and in the solid state and electrochemical properties. It was found that the bathochromic shift of the photoabsorption band from **4,4′-BBT** to **1,1′-Si-4,4′-BBT** and **1,1′,3,3′-Si-4,4′-BBT** is mainly attributed to the destabilization of the HOMO energy level through the introduction of the electron-donating *tert*-butyldimethylsilyl group into the benzo[*c*]thiophene skeleton, resulting in a decrease in the HOMO–LUMO band gap. The three 4,4′-bibenzo[*c*]thiophene derivatives exhibit moderate fluorescence properties in the solution (Φ_{fl} = *ca.* 0.4). Moreover, the silyl-substituted derivatives **1,1′-Si-4,4′-BBT** and **1,1′,3,3′-Si-4,4′-BBT** show relatively high $\Phi_{fl\text{-}solid}$ value (0.22 and 0.25, respectively) in the solid state, compared to **4,4′-BBT** ($\Phi_{fl\text{-}solid}$ < 0.02). The DFT calculations demonstrate that the HOMO energy levels of the 4,4′-bibenzo[*c*]thiophene derivatives are higher than that of benzo[*c*]thiophene (**BT**), while their LUMO energy levels are lower than that of **BT**. Consequently, this work opened up a new way for not only synthetic method and photophysical and electrochemical properties of 4,4′-bibenzo[*c*]thiophene derivatives with the different substituents on the thiophene rings, but also development of fused-bibenzo[*c*]thiophene derivatives as functional dyes.

Experimental

General

Melting points were measured with an AS ONE ATM-02. IR spectra were recorded on a SHIMADZU IRTracer-100 by ATR

method. ^{1}H NMR and ^{13}C NMR spectra were recorded on a Varian-500 FT NMR spectrometer and NMR solvent was used as an external standard for calibration. High-resolution mass spectral data by APCI and GC-EI were acquired on a Thermo Fisher Scientific LTQ Orbitrap XL and JEOL JMS-T100 GCV 4G, respectively. Recycling gel permeation chromatography (GPC) were preformed using RI-detector (GL Science RI 704) and pump (GILSON 307 PUMP) with column (Shodex GPC H-2001L). Photoabsorption spectra of solution were observed with a Shimadzu UV-3600 plus spectrophotometer. Photoabsorption spectra of the solid were recorded by a Shimadzu UV-3600 plus spectrophotometer with a calibrated integrating sphere system. Fluorescence spectra of solution and the solid were measured with a HORIBA FluoroMax-4 spectrofluorometer. The fluorescence quantum yields in solution and in the solid state were determined using a HORIBA FluoroMax-4 spectrofluorometer with a calibrated integrating sphere system. Fluorescence decay measurements were performed on a HORIBA DeltaFlex modular fluorescence lifetime system, using a Nano LED pulsed diode excitation source (370 nm). Cyclic voltammetry (CV) curves were recorded in acetonitrile/Bu_4NClO_4 (0.1 M) solution at a scan rate of 100 mV s^{-1} with a three-electrode system consisting of Ag/Ag^+ as the reference electrode, a Pt plate as the working electrode and a Pt wire as the counter electrode using an Electrochemical Measurement System HZ-7000 (HOKUTO DENKO).

Synthesis

4,4′-Bibenzo[*c*]thiophene (4,4′-BBT). To a THF solution (20 mL) of 1,1′,3,3′-tetrahydro-[4,4′-bibenzo[*c*]thiophene] 2,2′-dioxide (**1**)[20] (0.20 g, 0.66 mmol) under a nitrogen atmosphere at 0 °C was added dropwise a 1.3 M THF solution of lithium hexamethyldisilazide (3.1 mL, 4.0 mmol). After stirring for 3 h, the reaction mixture was quenched with water, and then, the solution was extracted with ethyl acetate. The ethyl acetate extract was dried over anhydrous $MgSO_4$, filtrated and concentrated. Recycling GPC (toluene as eluent) was performed to give **4,4′-BBT** (0.09 g, yield 51%) as a light-yellow solid; decomposed at around 145 °C; FT-IR (ATR): $\tilde{\nu}$ = 3103, 1686, 1172, 864 cm^{-1}; ^{1}H NMR (500 MHz, acetone-d_6): δ = 7.19–7.24 (m, 4H), 7.59 (dd, J = 1.1 and 3.4 Hz, 2H), 7.75 (dt, 2H), 8.00 (d, J = 3.4 Hz, 2H) ppm; ^{13}C NMR (125 MHz, acetone-d_6): δ = 117.96, 118.31, 122.51, 124.29, 124.35, 134.56, 138.45, 139.91 ppm; HRMS (GC-EI): m/z (%): [M − H$^+$] calcd for $C_{16}H_9S_2$, 265.01457; found 265.01442.

1,1′-Bis(*tert*-butyldimethylsilyl)-4,4′-bibenzo[*c*]thiophene (1,1′-Si-4,4′-BBT). (Method A: previous work)[20] To a THF solution (60 mL) of **1** (0.50 g, 1.65 mmol) under an argon atmosphere at −80 °C was added tetramethylethylenediamine (1.48 g, 9.92 mmol). After stirring for 30 min, a 1.6 M hexane solution of *n*BuLi (6.20 mL, 9.92 mmol) was added dropwise for 30 min, and then, a THF solution (10 mL) of *tert*-butyldimethylsilyl chloride (0.75 g, 4.96 mmol) was added dropwise for 20 min. After stirring for 12 h at room temperature, the reaction mixture was quenched with water, and then, the solution was extracted with ethyl acetate. The ethyl acetate extract was dried over anhydrous $MgSO_4$, filtrated and concentrated. The residue was chromatographed on silica gel (hexane as eluent), and then, recycling GPC (toluene as eluent) was performed to give **1,1′-Si-4,4′-BBT** (0.33 g, yield 40%) as a light-yellow solid. (Method B) To a THF solution (0.8 mL) of **4,4′-BBT** (0.14 g, 0.53 mmol) under a nitrogen atmosphere at 0 °C was added dropwise a 1.0 M hexane/THF solution of lithium diisopropylamide (1.6 mL, 1.6 mmol). After stirring for 3 h, a THF solution (0.3 mL) of *tert*-butyldimethylsilyl chloride (0.24 g, 1.6 mmol) was added dropwise. The reaction mixture was further stirred for 12 h. The reaction mixture was quenched with water, and then, the solution was extracted with ethyl acetate. The ethyl acetate extract was dried over anhydrous $MgSO_4$, filtrated and concentrated. The residue was chromatographed on silica gel (dichloromethane : hexane = 1 : 1 as eluent) and then on alumina (dichloromethane : hexane = 1 : 3 as eluent) to give **1,1′-Si-4,4′-BBT** (0.095 g, yield 36%) as a yellow solid; mp 153–155 °C; FT-IR (ATR): $\tilde{\nu}$ = 2949 (aliphatic C–H str.), 2926 (aliphatic C–H str.), 2855 (aliphatic C–H str.), 1458 (Si–C(Ar) str.), 1360, 1250 (aliphatic Si–CH_3 str.), 804 (aliphatic Si–CH_3 str.) cm^{-1}; ^{1}H NMR (500 MHz, $CDCl_3$): δ = 0.53 (s, 12H), 0.99 (s, 18H), 7.18–7.23 (m, 4H), 7.78 (d, J = 8.1 Hz, 2H), 7.81 (s, 2H) ppm; ^{13}C NMR (125 MHz, $CDCl_3$): δ = −3.73, 18.37, 26.92, 123.17, 123.25, 123.50, 124.03, 128.34, 134.88, 140.20, 145.12 ppm; HRMS (APCI): m/z (%): [M + H$^+$] calcd for $C_{28}H_{39}S_2Si_2$, 495.20262; found 495.20303.

1,1′,3,3′-Tetrakis(*tert*-butyldimethylsilyl)-4,4′-bibenzo[*c*]thiophene (1,1′,3,3′-Si-4,4′-BBT). (Method A) To a THF solution (0.8 mL) of **4,4′-BBT** (0.14 g, 0.53 mmol) under a nitrogen atmosphere at 0 °C was added dropwise a 1.0 M hexane/THF solution of lithium diisopropylamide (4.2 mL, 4.2 mmol). After stirring for 3 h, a THF solution (1.0 mL) of *tert*-butyldimethylsilyl chloride (0.62 g, 4.2 mmol) was added dropwise. The reaction mixture was further stirred for 12 h. The reaction mixture was quenched with water, and then, the solution was extracted with ethyl acetate. The ethyl acetate extract was dried over anhydrous $MgSO_4$, filtrated and concentrated. The residue was chromatographed on silica gel (dichloromethane : hexane = 1 : 3 as eluent) to give **1,1′,3,3′-Si-4,4′-BBT** (0.1 g, yield 26%) as a white solid. (Method B) To a THF solution (0.3 mL) of **1,1′-Si-4,4′-BBT** (0.07 g, 0.14 mmol) under a nitrogen atmosphere at 0 °C was added dropwise a 1.0 M hexane/THF solution of lithium diisopropylamide (1.4 mL, 1.4 mmol). After stirring for 3 h, a THF solution (0.3 mL) of *tert*-butyldimethylsilyl chloride (0.21 g, 1.4 mmol) was added dropwise. The reaction mixture was further stirred for 14 h. The reaction mixture was quenched with water, and then, the solution was extracted with dichloromethane. The dichloromethane extract was dried over anhydrous $MgSO_4$, filtrated and concentrated. The residue was chromatographed on silica gel (hexane as eluent) to give **1,1′,3,3′-Si-4,4′-BBT** (0.04 g, yield 40%) as a white solid; mp 172–173 °C; FT-IR (ATR): $\tilde{\nu}$ = 2955 (aliphatic C–H str.), 2926 (aliphatic C–H str.), 2855 (aliphatic C–H str.), 1470 (Si–C(Ar) str.), 1362, 1250 (aliphatic Si–CH_3 str.), 804 (aliphatic Si–CH_3 str.) cm^{-1}; ^{1}H NMR (500 MHz, acetone-d_6): δ = −0.87 (s, 3H), −0.04 (s, 3H), 0.57 (s, 3H), 0.62 (s, 3H), 0.77 (s, 9H), 0.99 (s, 9H), 7.02 (dd, J = 1.2 and 6.6 Hz, 2H), 7.19–7.22 (m, 2H), 7.99 (dd, J = 8.8 Hz, 2H) ppm; ^{13}C NMR (125

MHz, acetone-d_6): $\delta = -3.78, -3.61, 18.97, 19.32, 27.15, 28.25, 123.12, 125.27, 128.83, 136.01, 136.12, 139.28, 147.78, 149.76$ ppm; HRMS (APCI): m/z (%): [$M^{+\bullet}$] calcd for $C_{40}H_{66}S_2Si_4$, 722.36775; found 722.36843.

X-ray crystallographic analysis

The reflection data were collected at 100 K on a Bruker AXS SMART APEX II ULTRA diffractometer using monochromated Mo-Kα ($\lambda = 0.71073$ Å). The structure was solved by the SHELXT 2014/5 method and refined based on full-matrix least squares on F^2 using SHELXL-2017/1. The non-hydrogen atoms were refined anisotropically. Hydrogen atoms were fixed geometrically and not refined. Crystallographic data have been deposited in the Cambridge Crystallographic Data Centre (CCDC 2055734† for **1,1′-Si-4,4′-BBT** and CCDC 2055735† for **1,1′,3,3′-Si-4,4′-BBT**, respectively).

Crystal of 1,1′-Si-4,4′-BBT. A suitable single crystal of **1,1′-Si-4,4′-BBT** was grown by slow evaporation of acetone/ethanol solution at room temperature for several days, as colorless block crystal, air stable. Crystallographic data: $C_{28}H_{38}S_2Si_2$, $M = 494.88$, monoclinic, $a = 17.6427(9)$, $b = 11.2395(6)$, $c = 14.1794(7)$ Å, $\beta = 95.121(1)^\circ$, $V = 2800.5(2)$ Å^3, $D_{calcd} = 1.174$ g cm^{-3}, space group $P2_1/c$ (no. 14), $Z = 4$, 17 974 reflections measured, 6739 unique ($R_{int} = 0.027$), which were used in all calculations. The final R_1(reflections) = 0.0292(5949) [$I > 2\sigma(I)$], wR_2(reflections) = 0.0743(6739). GOF = 0.955 (Table S1†).

Crystal of 1,1′,3,3′-Si-4,4′-BBT. A suitable single crystal of **1,1′,3,3′-Si-4,4′-BBT** was grown by slow evaporation of acetone/ethanol solution at room temperature for several days, as colorless plate crystal, air stable. Crystallographic data: $C_{40}H_{66}S_2Si_4$, $M = 723.40$, triclinic, $a = 7.5572(9)$, $b = 13.6372(16)$, $c = 22.295(3)$ Å, $\alpha = 72.5230(10)^\circ$, $\beta = 89.9300(10)^\circ$, $\gamma = 81.0900(10)^\circ$, $V = 2162.7(4)$ Å^3, $D_{calcd} = 1.111$ g cm^{-3}, space group $P\bar{1}$ (no. 2), $Z = 2$, 10 428 reflections measured, 10 234 unique ($R_{int} = 0.041$), which were used in all calculations. The final R_1(reflections) = 0.0449(7519) [$I > 2\sigma(I)$], wR_2(reflections) = 0.1092(10 234). GOF = 1.011 (Table S1†).

Conflicts of interest

There are no conflicts to declare.

Acknowledgements

This work was supported by Grants-in-Aid for Scientific Research (B) from the Japan Society for the Promotion of Science (JSPS) KAKENHI Grant Number 19H02754.

Notes and references

1 M. E. Cinar and T. Ozturk, Thienothiophenes, Dithienothiophenes, and Thienoacenes: Syntheses, Oligomers, Polymers, and Properties, *Chem. Rev.*, 2015, **115**, 3036–3140.

2 J. Y. Kim, D. Yokoyama and C. Adachi, Horizontal Orientation of Disk-like Hole Transport Molecules and Their Application for Organic Light-Emitting Diodes Requiring a Lower Driving Voltage, *J. Phys. Chem. C*, 2012, **116**, 8699–8706.

3 (*a*) H. Usta, D. Kim, R. Ozdemir, Y. Zorlu, S. Kim, M. C. R. Delgado, A. Harbuzaru, S. Kim, G. Demirel, J. Hong, Y.-G. Ha, K. Cho, A. Facchetti and M.-G. Kim, High Electron Mobility in [1]Benzothieno[3,2-*b*][1]benzothiophene-Based Field-Effect Transistors: Toward n-Type BTBTs, *Chem. Mater.*, 2019, **31**, 5254–5263; (*b*) J. Li, L. Zheng, L. Sun, C. Li, X. Zhang, S. Cheng and W. Hu, New anthracene derivatives integrating high mobility and strong emission, *J. Mater. Chem. C*, 2018, **6**, 13257–13260.

4 (*a*) Y.-J. Cheng, S.-H. Yang and C.-S. Hsu, Synthesis of Conjugated Polymers for Organic Solar Cell Applications, *Chem. Rev.*, 2009, **109**, 5868–5923; (*b*) H. Tan, H. Tan, X. Zheng, J. Yang, J. Yu and W. Zhu, Significant influence of the benzothiophene ring substitution position on the photovoltaic performance of benzodithiophene-based donor polymers, *J. Mater. Chem. C*, 2020, **8**, 3183–3191; (*c*) J. Kim, H. Min Ko, N. Cho, S. Paek, J. K. Lee and J. Ko, Efficient small molecule organic semiconductor containing bis-dimethylfluorenyl amino benzo[*b*]thiophene for high open circuit voltage in high efficiency solution processed organic solar cell, *RSC Adv.*, 2012, **2**, 2692–2695.

5 (*a*) M. Liang and J. Chen, Arylamine organic dyes for dye-sensitized solar cells, *Chem. Soc. Rev.*, 2013, **42**, 3453–3488; (*b*) H. Choi, J. K. Lee, K. Song, S. O. Kang and J. Ko, Novel organic dyes containing bis-dimethylfluorenyl amino benzo [b]thiophene for highly efficient dye-sensitized solar cell, *Tetrahedron*, 2007, **63**, 3115–3121.

6 (*a*) K. Takimiya, I. Osaka, T. Mori and M. Nakano, Organic Semiconductors Based on [1]Benzothieno[3,2-*b*][1]benzothiophene Substructure, *Acc. Chem. Res.*, 2014, **47**, 1493–1502; (*b*) M. Nakano, I. Osaka, D. Hashizume and K. Takimiya, α-Modified Naphthodithiophene Diimides-Molecular Design Strategy for Air-Stable n-Channel Organic Semiconductors, *Chem. Mater.*, 2015, **27**, 6418–6425.

7 (*a*) F. Wudl, M. Kobayashi and A. J. Heeger, Poly(isothianaphthene), *J. Org. Chem.*, 1984, **49**, 3382–3384; (*b*) K. Kobayashi, N. Colaneri, M. Boysel, F. Wudl and A. J. Heeger, The electronic and electrochemical properties of poly(isothianaphthene), *J. Chem. Phys.*, 1985, **82**, 5717–5723; (*c*) R. Lazzaroni, J. Riga, J. Verbist, J. L. Brédas and F. Wudl, *J. Chem. Phys.*, 1988, **88**, 4257–4262; (*d*) H. Meng and F. Wudl, A Robust Low Band Gap Processable n-Type Conducting Polymer Based on Poly(isothianaphthene), *Macromolecules*, 2001, **34**, 1810–1816.

8 (*a*) S. T. Meek, E. E. Nesterov and T. M. Swager, Near-Infrared Fluorophores Containing Benzo[*c*]heterocycle Subunits, *Org. Lett.*, 2008, **10**, 2991–2993; (*b*) A. K. Mohanakrishnan and P. Amaladass, Synthesis of 1,3-diaryl benzo[*c*]thiophenes, *Tetrahedron Lett.*, 2005, **46**, 4225–4229; (*c*) K. Kawabata and H. Goto, Synthesis and optical properties of 1,1-binaphthyl–thiophene alternating copolymers with main chain chirality, *J. Mater. Chem.*, 2012, **22**, 23514–23524; (*d*) J. A. Clement, P. Gunasekaran and A. K. Mohanakrishnan, Synthesis and characterization of benzo[*c*]thiophene

analogs incorporating benzo[*b*]thiophene/1-hexylindole/benzo[*b*]furan, *Tetrahedron*, 2009, **65**, 4113–4123; (*e*) S. Ogawa, H. Muraoka, K. Kikuta, F. Saito and R. Sato, Design of reversible multi-electron redox systems using benzochalcogenophenes containing aryl and/or ferrocenyl fragments, *J. Organomet. Chem.*, 2007, **692**, 60–69.

9 (*a*) G. G. Rajeshwaran, M. Nandakumar, R. Sureshbabu and A. K Mohanakrishnan, Lewis Acid-Mediated Michaelis–Arbuzov Reaction at Room Temperature: A Facile Preparation of Arylmethyl/Heteroarylmethyl Phosphonates, *Org. Lett.*, 2011, **13**, 1270–1273; (*b*) Y. Qin, J. Y. Kim, C. D. Frisbie and M. A. Hillmyer, Distannylated Isothianaphthene: A Versatile Building Block for Low Bandgap Conjugated Polymers, *Macromolecules*, 2008, **41**, 5563–5570; (*c*) R. A. Kumar, M. R. Pattanayak, E. Yen-Pon, J. Eliyan, K. Porte, S. Bernard, M. Riomet, P. Thuéry, D. Audisio and F. Taran, Strain-Promoted 1,3-Dithiolium-4-olates–Alkyne Cycloaddition, *Angew. Chem., Int. Ed.*, 2019, **58**, 14544–14548; (*d*) M. R. Raj and S. Anandan, Donor conjugated polymers-based on alkyl chain substituted oligobenzo[*c*]thiophene derivatives with well-balanced energy levels for bulk heterojunction solar cells, *RSC Adv.*, 2013, **3**, 14595–14608; (*e*) T. J. L. Silva, P. J. Mendes, M. H. Garcia, M. P. Robalo, J. P. P. Ramalho, A. J. P. Carvalho, M. Büchert, C. Wittenburg and J. Heck, Benzo[*c*]thiophene Chromophores Linked to Cationic Fe and Ru Derivatives for NLO Materials: Synthesis Characterization and Quadratic Hyperpolarizabilities, *Eur. J. Inorg. Chem.*, 2013, 3506–3517.

10 (*a*) N. S. Kumar and A. K. Mohanakrishnan, Synthesis and characterization of fluorene tethered benzo[*c*]thiophene/benzo[*c*]selenophene analogs, *Tetrahedron*, 2010, **66**, 5660–5670; (*b*) R. Sivasakthikumaran, J. A. Clement, M. Nandakumar and A. K. Mohanakrishnan, Synthesis and Characterization of Thienothiophene Conjugated Benzo[*c*] Thiophene Analogs, *J. Heterocycl. Chem.*, 2016, **53**, 1461–1468; (*c*) R. D. A. Hudson, I. Asselberghs, K. Clays, L. P. Cuffe, J. F. Gallagher, A. R. Manning, A. Persoons and K. Wostyn, The linear and nonlinear optical properties of organometallic chromophores derived from ferrocene, $[Fe_2(\eta^5\text{-}C_5H_5)_2(CO)_2(\mu\text{-}CO)(\mu\text{-}C\text{–}CH_3)]^+[BF_4]^-$ and terthienyl spacers. Crystal structure of 2-[(*E*)-2-ferrocenylethenyl]-5-(2-thienyl)thiophene, *J. Organomet. Chem.*, 2001, **637–639**, 435–444; (*d*) W. Debrouwer, R. A. J. Seigneur, T. S. A. Heugebaert and C. V. Stevens, Gold superacid-catalyzed preparation of benzo[*c*]thiophenes, *Chem. Commun.*, 2015, **51**, 729–732; (*e*) R. Sato, E. Takeda, S. Nakajo, T. Kimura, S. Ogawa and Y. Kawai, Oxidation of 1,4-dihydro-1,4-diphenyl-2,3-benzodithiin, *Heteroat. Chem.*, 2001, **12**, 209–216; (*f*) R. Kiebooms, I. Hoogmartens, P. Adriaensens, D. Vanderzande and J. Gelan, Low-Band-Gap Conjugated Polymers. Improved Model Compounds for the Structural Analysis of Poly(isothianaphthene), *Macromolecules*, 1995, **28**, 4961–4969.

11 (*a*) U. Mitschke and P. Bäuerle, Synthesis, characterization, and electrogenerated chemiluminescence of phenyl-substituted, phenyl-annulated, and spirofluorenyl-bridged oligothiophenes, *J. Chem. Soc., Perkin Trans. 1*, 2001, 740–753; (*b*) R. Kisselev and M. Thelakkat, Synthesis and Characterization of Poly(triarylamine)s Containing Isothianaphthene Moieties, *Macromolecules*, 2004, **37**, 8951–8958; (*c*) T. V. Hughes and M. P. Cava, Electrophilic Cyanations Using 1-Cyanobenzotriazole: sp^2 and sp Carbanions, *J. Org. Chem.*, 1999, **64**, 313–315; (*d*) V. Dhayalan, J. A. Clement, R. Jagan and A. K. Mohanakrishnan, A Versatile Synthesis of Annulated Carbazole Analogs Involving a DominoReaction of Bromomethylindoles with Arenes/Heteroarenes, *Eur. J. Org. Chem.*, 2009, 531–546; (*e*) K. Willinger, K. Fischer, R. Kisselev and M. Thelakkat, Synthesis, spectral, electrochemical and photovoltaic properties of novel heteroleptic polypyridyl ruthenium(II) donor-antenna dyes, *J. Mater. Chem.*, 2009, **19**, 5364–5376; (*f*) M. Hori, T. Kataoka, H. Shimizu, J. Hongo and M. Kido, Reactions of 1*H*-2-benzothiopyran 2-oxides with active methylene compounds: a novel ring contraction of 1-aryl derivatives to benzo[*c*]thiophenes. X-Ray molecular structure of 1-(2,2-diacetylvinyl)-3-phenylbenzo[*c*]thiophene, *J. Chem. Soc., Perkin Trans. 1*, 1989, 1611–1618.

12 (*a*) M. Usui, H. Fukumoto and T. Yamamoto, Synthesis of New Thiperkinophene-Based π-Conjugated Organic Compounds and Polymer, *Bull. Chem. Soc. Jpn.*, 2010, **83**, 1397–1399; (*b*) Q. Liu, Q.-Y. Feng, H. Yamada, Z.-S. Wang, N. Ono, X.-Z. You and Z. Shen, Tuning the Spectroscopic, Electrochemical, and Photovoltaic Properties of Triaryl Amine Based Sensitizers through Ring-Fused Thiophene Bridges, *Chem.–Asian J.*, 2012, **7**, 1312–1319; (*c*) A. K. Mohanakrishnan, J. A. Clement, P. Amaladass and V. S. Thirunavukkarasu, Synthesis of 1,3-disubstituted benzo[*c*]thiophene analogs containing benzo[*b*]thiophene/benzo[*b*]pyrrole, *Tetrahedron Lett.*, 2007, **48**, 8715–8720; (*d*) A. K. Mohanakrishnan, N. S. Kumar and P. Amaladass, Synthesis and characterization of 9,9-dialkylfluorene capped benzo[*c*]thiophene/benzo[*c*]selenophene analogs as potential OLEDs, *Tetrahedron Lett.*, 2008, **49**, 4792–4795; (*e*) N. S. Kumar, J. A. Clement and A. K. Mohanakrishnan, Synthesis and characterization of benzo[*c*]thiophene analogs tethered with dibenzo-heterocycles as potential OLEDs, *Tetrahedron*, 2009, **65**, 822–830; (*f*) R. H. L. Kiebooms, P. J. A. Adriaensens, D. J. M. Vanderzande and J. M. J. V. Gelan, Grignard Reactions on Ortho Dicarboxylic Arene Derivatives. Synthesis of 1,3-Dithienylisothianaphthene Compounds, *J. Org. Chem.*, 1997, **62**, 1473–1480.

13 (*a*) J. D. Douglas, G. Griffini, T. W. Holcombe, E. P. Young, O. P. Lee, M. S. Chen and J. M. J. Fréchet, Functionalized Isothianaphthene Monomers That Promote Quinoidal Character in Donor–Acceptor Copolymers for Organic Photovoltaics, *Macromolecules*, 2012, **45**, 4069–4074; (*b*) J. W. Terpstra and A. M. van Leusen, A new synthesis of benzo[*b*]thiophenes and benzo[*c*]thiophenes by annulation of disubstituted thiophenes, *J. Org. Chem.*, 1986, **51**, 230–238; (*c*) R. M. El-Shishtawy, K. Fukunishi and S. Miki, Synthesis and photoreaction of 4,5,7-tri-*t*-butyl benzo[*c*]

thiophene: A novel benzo[c]thiophene derivative and its Dewar isomer, *Tetrahedron Lett.*, 1995, **36**, 3177–3180; (*d*) J. C. Throgmorton, S. M. Chintala and R. D. McCulla, Synthesis of Unsymmetric Monosubstituted and Disubstituted Dinaphthothiophenes, *J. Heterocycl. Chem.*, 2017, **54**, 3682–3688.

14 (*a*) K. Yamamoto, Y. Ie, M. Nitani, N. Tohnai, F. Kakiuchi, K. Zhang, W. Pisula, K. Asadi, P. W. M. Blom and Y. Aso, Oligothiophene quinoids containing a benzo[*c*]thiophene unit for the stabilization of the quinoidal electronic structure, *J. Mater. Chem. C*, 2018, **6**, 7493–7500; (*b*) K. Fukuzumi, Y. Unoh, Y. Nishii, T. Satoh, K. Hirano and M. Miura, Synthesis of Benzo[*c*]thiophenes by Rhodium(III)-Catalyzed Dehydrogenative Annulation, *J. Org. Chem.*, 2016, **81**, 2474–2481; (*c*) Y.-C. Hu, Z.-L. Lin, T.-C. Huang, J.-W. Lee, W.-C. Wei, T.-Y. Ko, C.-Y. Lo, D.-G. Chen, P.-T. Chou, W.-Y. Hung and K.-T. Wong, New exciplex systems composed of triazatruxene donors and *N*-heteroarene-cored acceptors, *Mater. Chem. Front.*, 2020, **4**, 2029–2039; (*d*) K. Kobayashi, Y. Honda and Y. Shigemura, An Efficient Synthesis of 1-Arylbenzo[*c*]thiophenes *via* the Reaction of 2-(Chloromethyl)phenyllithiums with Aromatic Aldehydes, *Heterocycles*, 2017, **94**, 1707–1717; (*e*) C. P. Yu, R. Kimura, T. Kurosawa, E. Fukuzaki, T. Watanabe, H. Ishii, S. Kumagai, M. Yano, J. Takeya and T. Okamoto, Air-Stable Benzo[*c*]thiophene Diimide n-Type π-Electron Core, *Org. Lett.*, 2019, **21**, 4448–4453.

15 (*a*) D.-T. Hsu and C.-H. Lin, Synthesis of Benzo[*c*] and Naphtho[*c*]heterocycle Diesters and Dinitriles *via* Homoelongation, *J. Org. Chem.*, 2009, **74**, 9180–9187; (*b*) W. A. Braunecker, S. D. Oosterhout, Z. R. Owczarczyk, R. E. Larsen, B. W. Larson, D. S. Ginley, O. V. Boltalina, S. H. Strauss, N. Kopidakis and D. C. Olson, Ethynylene-Linked Donor–Acceptor Alternating Copolymers, *Macromolecules*, 2013, **46**, 3367–3375; (*c*) A. Ishii, J. Nakayama, J. Kazami, Y. Ida, T. Nakamura and M. Hoshino, Synthesis and reactions of 1,3,4,6-tetra-2-thienylthieno[3,4-*c*]thiophene, *J. Org. Chem.*, 1991, **56**, 78–82; (*d*) G. M. Brooke and S. D. Mawson, Partially fluorinated heterocyclic compounds. Part 27. The synthesis of 4,5,6,7-tetrafluorobenzo[*c*]thiophene and 4,5,6,7,8,9-hexafluoronaphtho-[1,2-*c*]thiophene; some chemistry and electrochemistry, *J. Chem. Soc., Perkin Trans. 1*, 1990, 1919–1923.

16 (*a*) T. Saito, H. Ayukawa, N. Sumizawa, T. Shizuta, S. Motoki and K. Kobayashi, Reaction of aryl biphenyl-2-yl thioketones with ditosyldiazomethane; internal cyclisation of the thioketone *S*-methylides to afford benzo[*c*]thiophene derivatives. Structure determination of the products by Raney nickel degradation and X-ray crystallographic analysis, *J. Chem. Soc., Perkin Trans. 1*, 1991, 1405–1410; (*b*) R. R. Amaresh, M. V. Lakshmikantham, J. W. Baldwin, M. P. Cava, R. M. Metzger and R. D. Rogers, Condensed Thiophenes and Selenophenes: Thionyl Chloride and Selenium Oxychloride as Sulfur and Selenium Transfer Reagents, *J. Org. Chem.*, 2002, **67**, 2453–2458; (*c*) D. Rajagopal, M. V. Lakshmikantham, E. H. Mørkved and M. P. Cava, Generation of the First Tellurium-Containing Diheteropentalene, *Org. Lett.*, 2002, **4**, 1193–1195; (*d*) N. Yasmin, M. Ghosh and J. K. Ray, P_4S_{10} and Na_2S-mediated novel annulation routes to *c*-fused thiophenes, *RSC Adv.*, 2014, **4**, 19932–19938.

17 (*a*) Y. Okuda, M. V. Lakshmikantham and M. P. Cava, A new route to 1,3-disubstituted benzo[*c*]thiophenes, *J. Org. Chem.*, 1991, **56**, 6024–6026; (*b*) E. Aqad, M. V. Lakshmikantham and M. P. Cava, *N*,*N*-Dimethylformamide-Mediated Sodium Reduction of *trans*-3,3′-Benzo[*c*]thienylidene-1,1′-dithione and *trans*-3,3′-Benzo[*c*]selenonylidene-1,1′-dithione, *Org. Lett.*, 2004, **6**, 3039–3041.

18 (*a*) A. K. Mohanakrishnan, P. Amaladass and J. A. Clement, Synthesis of end-blocked thienyl oligomers incorporating benzo[*c*]thiophene, *Tetrahedron Lett.*, 2007, **48**, 779–784; (*b*) P. Amaladass, J. A. Clement and A. K. Mohanakrishnan, Synthesis and Characterization of Benzannelated Thienyl Oligomers, *Eur. J. Org. Chem.*, 2008, 3798–3810.

19 (*a*) Y. Shimizu, Z. Shen, S. Ito, Hi. Uno, J. Daub and N. Ono, A convenient synthesis of isothianaphthene oligomers and theirelectrochemical studies, *Tetrahedron Lett.*, 2002, **43**, 8485–8488; (*b*) Q. Liu, F.-T. Kong, T. Okujima, H. Yamada, S.-Y. Dai, H. Uno, N. Ono, X.-Z. You and Z. Shen, Synthesis and spectroscopic properties of ring-fused thiophene bridged push–pull dyes and their application in dye-sensitized solar cells, *Tetrahedron Lett.*, 2012, **53**, 3264–3267.

20 Y. Ooyama, T. Enoki, S. Aoyama and J. Ohshita, Synthesis and optical and electrochemical properties of a phenanthrodithiophene (fused-bibenzo[*c*]thiophene) derivative, *Org. Biomol. Chem.*, 2017, **15**, 7302–7307.

21 (*a*) H. Langhals, T. Potrawa, H. Nöth and G. Linti, The Influence of Packing Effects on the Solid-State Fluorescence of Diketopyrrolopyrroles, *Angew. Chem., Int. Ed.*, 1989, **28**, 478–480; (*b*) H.-C. Yeh, W.-C. Wu, Y.-S. Wen, D.-C. Dai, J.-K. Wang and C.-T. Chen, Derivative of α,β-Dicyanostilbene: Convenient Precursor for the Synthesis of Diphenylmaleimide Compounds, *E*–*Z* Isomerization, Crystal Structure, and Solid-State Fluorescence, *J. Org. Chem.*, 2004, **69**, 6455–6462; (*c*) Y. Ooyama, T. Okamoto, T. Yamaguchi, T. Suzuki, A. Hayashi and K. Yoshida, Heterocyclic Quinol-Type Fluorophores: Synthesis, X-ray Crystal Structures, and Solid-State Photophysical Properties of Novel 5-Hydroxy-5-substituent-benzo[*b*]naphtho[1,2-*d*]furan-6-one and 3-Hydroxy-3-substituent-benzo[*kl*]xanthen-2-one Derivatives, *Chem.–Eur. J.*, 2006, **12**, 7827–7838; (*d*) Y. Ooyama, Y. Hagiwara, Y. Oda, H. Fukuoka and J. Ohshita, BODIPY dye possessing solid-state red fluorescence and green metallic luster properties in both crystalline and amorphous states, *RSC Adv.*, 2014, **4**, 1163–1167.

22 Both the geometry optimization and energy calculation were performed by employing the density functional theory (DFT), at the level of B3LYP/6-31G(d,p) on the Gaussian 16 program package:M. J. Frisch, G. W. Trucks, H. B. Schlegel, G. E. Scuseria, M. A. Robb, J. R. Cheeseman, G. Scalmani, V. Barone, G. A. Petersson, H. Nakatsuji, X. Li, M. Caricato, A. V. Marenich, J. Bloino, B. G. Janesko, R. Gomperts,

B. Mennucci, H. P. Hratchian, J. V. Ortiz, A. F. Izmaylov, J. L. Sonnenberg, D. Williams-Young, F. Ding, F. Lipparini, F. Egidi, J. Goings, B. Peng, A. Petrone, T. Henderson, D. Ranasinghe, V. G. Zakrzewski, J. Gao, N. Rega, G. Zheng, W. Liang, M. Hada, M. Ehara, K. Toyota, R. Fukuda, J. Hasegawa, M. Ishida, T. Nakajima, Y. Honda, O. Kitao, H. Nakai, T. Vreven, K. Throssell, J. A. Montgomery, Jr., J. E. Peralta, F. Ogliaro, M. J. Bearpark, J. J. Heyd, E. N. Brothers, K. N. Kudin, V. N. Staroverov, T. A. Keith, R. Kobayashi, J. Normand, K. Raghavachari, A. P. Rendell, J. C. Burant, S. S. Iyengar, J. Tomasi, M. Cossi, J. M. Millam, M. Klene, C. Adamo, R. Cammi, J. W. Ochterski, R. L. Martin, K. Morokuma, O. Farkas, J. B. Foresman, and D. J. Fox, *Gaussian 16, Revision B.01*, Gaussian, Inc., Wallingford CT, 2016.